ISSN 1648-4142 / eISSN 1648-3480

VILNIUS TECH
Vilnius Gediminas Technical University

TRANSPORT

2024
Volume 39
Issue 2
Pages 183–196
https://doi.org/10.3846/transport.2024.22411

Original Article

EXAMINING FAILURES IN RUBBER-CORD COUPLINGS WITHIN ER2 SERIES ELECTRIC TRAINS

Pavels GAVRILOVS✉, Dmitrijs GORBACOVS, Janis EIDUKS, Guntis STRAUTMANIS, Ali ARSHAD

Dept of Railway Engineering, Faculty of Mechanical Engineering, Transport and Aeronautics, Riga Technical University, Latvia

Highlights:

- rubber-cord couplings installed on EMUs in operation are affected by forces and moments acting on them, and they also subject to the impact of temperature, as a result, rubber-cord couplings may fail;
- failure of a rubber-cord coupling results in unscheduled repairs;
- the replacing of rubber-cord coupling it is a labour-intensive and expensive process;
- the consequences of a rubber-cord coupling failure may lead to a disruption of the train traffic;
- using various research methods, for different factors the causes of rubber-cord couplings failures were found, based on the results of the studies, recommendations were given, the implementation of which will reduce the number of rubber-cord couplings failures.

Article History:

- submitted 14 November 2022;
- resubmitted 26 November 2023;
- accepted 5 December 2023.

Abstract. The article provides statistics on failures of rubber-cord couplings of electric trains of the ER2 and ER2T series and of the diesel trains over the past 7 years. According to statistics, over the past 7 years, 107 rubber-cord couplings have failed. Of these, the largest number of cases of failure of rubber-cord couplings occurred on rolling stock of the ER2 series. Examining failed rubber-cord couplings, it was revealed that the cause of its failure was a rupture of the side surface. Replacing a rubber-cord coupling is a labour-intensive and costly process. Accordingly, the question arises: what causes the problem and what measures should be proposed to reduce the failures. For these purposes, the work presents a number of experiments in order to identify possible causes of failure of the rubber-cord coupling. The article presents studies of the heating temperature of rubber-cord couplings in operation on motor cars, as well as a number of studies of failed rubber-cord couplings removed from motor cars. During the research, such parameters as the date of the last repair and the date of failure of the rubber-cord coupling were taken into account. The number of days the motor car was in general operation was taken into account until the failure of the rubber-cord coupling, as well as the mileage of the motor car after the repair. Measurements were carried out of the geometric parameters of the rubber-cord coupling: outer and inner diameter, thickness of the side of the rubber-cord coupling. The torque of the rubber-cord coupling acting at speeds from 5 to 40 km/h, the forces acting in operation on the rubber-cord coupling were calculated, and torsional and shear stresses were also studied and determined. Research was carried out to determine the hardness of the rubber-cord coupling in the temperature range from –20 °C to 0 °C and from 0 °C to +22 °C, as well as from +22 °C to +60 °C. These parameters were taken since a rubber-cord coupling operates under the mentioned conditions. In conclusion, possible reasons for the failure of rubber-cord couplings are given, and recommendations for reduction of their frequency are proposed.

Keywords: train, traction gear, rubber-cord coupling, forces and stresses in rubber, Shore A, temperature, electric trains failures.

✉Corresponding author. E-mail: *pavels.gavrilovs@rtu.lv*

Notations

CB – carbon black;
DC – direct current;
DR1A – Riga diesel train 1 type;
EMU – electric multiple unit;
ER2, ER2T – DC EMU;
NR – natural rubber;
SBR – styrene butadiene rubber;
SIR – silicone rubber;
TR-3 – type 3 scheduled repair.

1. Introduction

The rubber-cord coupling is used to transfer torque from the traction motor shaft to the wheelset gearbox (Cukalo, Prosvirin 1994) and is attached on one side to the traction motor shaft flanges, and on the other side – by bolts to the traction gearbox small gear shaft flange. According to the repair rules (VAS LD 1997) M24 bolts with a conditional strength of 10.9 shall be used. The design of the coupling is shown on Figure 1.

The use of rubber-cord couplings makes it possible to smooth out the dynamic loads from the track superstructure perceived by the traction gear and makes the rolling stock run smoothly (Pegov *et al.* 2003). The rubber-cord coupling, under proper operating conditions and small mutual displacements of the connected shafts, is characterized by an increased reliability. However, in the conditions of suburban traffic with a different range of speeds from 0 to 120 km/h, in combination with a large occupancy of the motor car during the morning and evening peaks of passenger transportation, as well as in the summer, as a result of the subsidence of the motor car, the traction drive shaft and the traction motor shaft is subjected to significant misalignment, and the greater the displacement of the shafts, the greater the forces acting on the coupling, and accordingly, the rubber-cord coupling will have a shorter service life. In addition, during the movement of the electric train, various forces and moments act on the rubber-cord coupling, related to the speed and operation mode of the train (traction, coasting, braking). As a result, cyclic stresses arise in the material of the rubber-cord coupling, which also cause its warming, which is especially manifested in the summer season. In addition, in the conditions of the Latvian railway, the coupling operates in a broad temperature range from –20 °C in winter to +30 °C in summer. Such temperature range also affects the mechanical properties and the hardness of the coupling material, and as a result of the influence of high temperature, its aging. As a result of all the above factors, the properties of rubber may deteriorate, and cracks and breaks may occur in the material of the rubber-cord coupling, which are significant shear stress concentrators, as a result of which the coupling may fail.

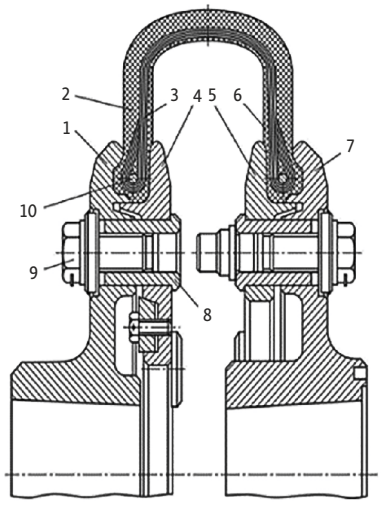

Figure 1. Section view of the ER2 series electric train rubber-cord coupling:
1, 7 – flange; 2 – protector; 3 – rubber-cord frame; 4, 5 – internal fastening semi-disc; 6 – inner protective layer; 8 – mounting sleeve; 9 – mounting bolt M24; 10 – metal ring

Rubber-cord couplings operate under dynamic load conditions with high force and vibration loads. Generally, the rubber-cord coupling during operation is affected by external atmospheric factors: water, dust, solid particles, reduced air humidity and temperature. Aggressive substances, such as lubricants, oils, chemical liquids, also get onto the coupling from the sides of the aggregates. These factors cause accelerated hardening or softening of rubber, cracking, which reduces the deforming properties of the coupling and their service life (Korneev *et al.* 2016). Fixing of the rubber-cord coupling takes place by compressing the walls of the case with steel flanges, using screws. In such a joint, loosening of the joint is possible and, as a result, slippage between the shell and the flanges, which causes overheating of the shell or mechanical damage of the shell.

Analysis of statistical data on the failure of rubber-cord couplings on the rolling stock used on the Latvian Railway over the past 7 years from 2015 to 2021 showed that 107 cases of failure occurred on electric trains, of which 66 cases on of the trains of the ER2 series and 35 cases on the ER2T series; for the diesel trains, failure of the rubber-cord coupling amounted only to 6 cases (AS PV 2021). Failure statistics are shown in Figure 2.

Many authors have studied the issue of rubber aging. The authors investigated the effect of radiation-humidity aging on the thermodynamic and interfacial properties of nanosilicate/SIR composites using molecular dynamic modelling (Lou *et al.* 2023).

Due to the fact that rubber is rubber, there is a lot of research in this area. In the work study on the fatigue resistance of NR with SiO_2 microspheres different silane coupling agents were used for modification of N98 through wet mixing process. The results in this works show that N98@KH570 powder has no effect on the curing property, tensile property and wear resistance of NR/N98 composites, but can increase the viscosity of Mooney, reduce the tear strength, and slightly increase the hardness of NR/N98 composites (Zhou *et al.* 2023).

In the work failure, characterization of SIR in corrosive environments based on leakage current characteristics authors discusses the failure properties of HTV SIR in different energized corrosive environments and explores the characteristics that can characterize insulation failure. The findings demonstrate that the leakage current characteristics (the maximum values, the number of characteristic pulses, and cumulative charge) can effectively characterize the surface state of SIR in corrosive environments. A failure characterization method of SIR based on the proportion of pulse number and cumulative discharge is proposed in

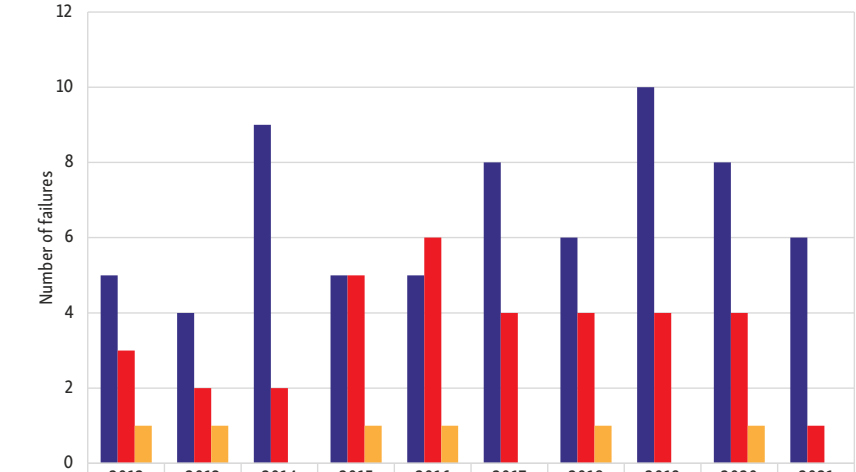

	2012	2013	2014	2015	2016	2017	2018	2019	2020	2021
ER2	5	4	9	5	5	8	6	10	8	6
ER2T	3	2	2	5	6	4	4	4	4	1
DR1A	1	1	0	1	1	0	1	0	1	0

Figure 2. EMU rubber-cord coupling failures

this article. The findings are helpful in forecasting pollution flashovers and insulation failure in heavy fog, coastal, and industrial pollution areas (Zhang *et al.* 2023).

In the work studies on swelling behaviour, mechanical and thermal properties of ternary rubber blend composites in the presence of compatibilizers the authors study the swelling, mechanical and thermal properties of ternary rubber composites obtained by melt mixing NR with CB/SBR/nitrile butadiene rubber in a melt. The authors proved that compatibilizers significantly improve the properties of the resulting composites when loading the studied compatibilizers due to uniform dispersion of CB in a rubber matrix. The use of compounds in the rubber industry has led to highly efficient production of low-cost products. Rubber compounds have a significant positive impact on a wide range of applications, such as construction, aerospace, military, packaging, tires and biomedicine, so improving the compatibility of mixtures will make new materials suitable for new applications (Abdelsalam *et al.* 2023).

In the work rubber aging life prediction based on interpolation and improved time-temperature superposition principle an accurate prediction and assessment of the deterioration of rubber characteristics during aging at room temperature is investigated, it is proposed to calculate the pseudo-failure period at each different acceleration temperature by the interpolation method based on data on accelerated aging in the room at high temperatures and on the basis of the resulting pseudo-failure resource. In the work rubber aging life prediction based on interpolation and improved time-temperature superposition principle an accurate prediction and assessment of the deterioration of rubber characteristics during aging at room temperature is investigated, it is proposed to calculate the pseudo-failure period at each different acceleration temperature by the interpolation method based on data on accelerated aging in the room at high temperatures and on the basis of the resulting pseudo-failure resource (Li *et al.* 2022).

2. Literature review

During the operation the mechanical equipment of the EMU train experiences dynamic loads arising under the action of unbalanced forces and moments caused by unsteady movement of the rotating masses of the running EMU train traction drive. The action of unbalanced forces and moments leads to the occurrence of cyclic stresses in the rubber-cord coupling, due to which the coupling may fail. Operational experience of traction drives shows that in terms of durability, rubber-cord couplings are one of the weak links, as they experience pulsed alternating, high-frequency periodic and non-periodic loads in traction transmissions of EMU trains.

Rubber-cord coupling refers to rubber-cord torus-shaped coupling shells of connecting devices of railway rolling stock power drives and other similar devices in the field of mechanical engineering, and can be used to transmit torque with significant angular, axial, radial displacements of shafts (Pegov *et al.* 2003).

In the work dynamics of moving coupled objects with stabilizers and unconventional couplings a comprehensive investigation was carried out to analyse the vibration stability of a coupled bogie system moving uniformly along a complexly modelled flexibly supported infinite high-order shear deformable coupled beam system on a viscoelastic base. The main contribution of this study involves a comparative analysis of the specific coupling of the bogie system with and without the proposed additional stabilizer, in comparison to conventional cases. The study demonstrates significant benefits of the newly proposed options of dual coupling and additional stabilizers in terms of stability. Another contribution of the study is the feasibility of the proposed unconventional models in technical practice. A phenomenon has been discovered that increasing the viscous damping in a special coupling leads to the occurrence of motion instability in the mechanical system. The

article also presents a novel technical solution for connecting moving objects at high speeds. The benefits of the additional oscillator as a stabilizer are extensively illustrated through numerous different examples. The bogie is specifically connected to another bogie in 2 new ways: with an additional stabilizer allowing double transverse displacement and providing an additional contact with the base, or with a specific coupling that enables simultaneous rotational and transverse displacement at the contact point. The analysis reveals 2 key findings. 1st, the additional mechanical stabilizer allows for the widest range of permissible suspension stiffness (largest stability region) when the connection is conventional. 2nd, enabling transverse displacement in the couplings results in a stable regime of motion at much lower suspension stiffness compared to other cases (Stojanović *et al.* 2024).

With the development of new production technologies, rubber-cord couplings are increasingly used in many areas of industry, as well as at marshalling yards (Ischuka *et al.* 2019, 2020). There are various designs of rubber-cord couplings that are used in pneumatic damping systems and means of protection against shock and vibration levels in the railway turnouts' drives (Muhitovs *et al.* 2020).

In the publication dynamic loading reduction and specific features of force drives operation for normal and abnormal conditions the experimental results are presented on the study of dynamic loading of the force drives of a railroad rolling stock in nominal and maximum loadings. The graphics of comparative investigation are given for the drive elements with elastic coupling and rigid joint. It is shown that using the rubber-cord shells in joining devices reduces the torsional oscillations in force drives (Mahutov *et al.* 2005).

In the publication by Ahundov & Lunev (2011), the calculation and experimental results of twisting of EMU trains rubber-cord coupling shells are reflected. The type of cord and parameters of reinforcement, at which a shell possesses necessary twisting moment dependence on the twist angle is presented.

Sheshenin *et al.* (2021) were engaged in the study and determination of the viscoelastic properties of the rubber-cord layer in a plane stress state. This work is devoted to determining the relaxation functions of rubber and rubber-cord.

An article experimental stand to study the load characteristics of a rubber-cord flat is devoted to the computational and experimental study of rubber-cord flat couplings, which allow the transmission of large torques; such couplings are distinguished by their simplicity of design, the absence of frictional surfaces and axial forces (when loaded with torque), insensitivity to dust and moisture; they facilitate reduction of vibration and noise levels (Il'ichev *et al.* 2015). Rubber-cord flat couplings also have high compensating properties, which allows them to be used with significant radial, axial and angular displacements of the connected shafts in drives experiencing static and dynamic loads in a wide range of values. In another article by this author is given a description of a specially designed experimental test bench and a method for determining the load characteristics of a rubber-cord disk (plate) for highly elastic couplings.

Analysing the above studies by international authors, we can conclude that in these scientific articles the authors did not consider such issues as measuring the hardness of the coupling material at different temperatures –20 °C; 0 °C; +22 °C; +60 °C, the measurement of the geometric parameters of the rubber-cord coupling was not taken into account. The stresses acting on the coupling were not studied, and the lateral surface of the coupling was not tested for tensile strength. Such important indicators as the determination of tangential torsional shear stresses were not determined. The articles also do not provide statistics on failures of rubber-cord couplings, whether this problem is an urgent topic. Accordingly, the question arises and the main goal of the work is how the above parameters affect the reliability of operation and what are the main possible reasons for the rupture of the side surface of the rubber-cord coupling. In the article, the authors decided to investigate this problem.

3. Experimental methods

The rubber-cord coupling damage is one of the main problems that lead to failure of the electric trains traction gear. Over the past 7 years, 208 cases of unscheduled repairs of motor cars of ER2 series trains due to failures of traction gear have been identified. Of these, in 48 cases, the side surface of the rubber-cord coupling ruptured (AS PV 2021). Accordingly, this is 20% of the total number of traction gear failures. Analysis of statistical data is shown on Figure 3.

The graph (Figure 3) shows the total number of unscheduled repairs of the traction gear of the ER2 series EMU trains, in comparison with the number of unscheduled repairs of the traction gear due to a rupture of the rubber-cord coupling shell. When ascertaining a rupture of the coupling shell, the motor car of the ER2 series EMU train needs to undergo unscheduled repair related to the replacement of the rubber-cord couplings. Data on financial costs caused by such unscheduled repairs for various rolling stock is presented in Table 1.

The results of a visual inspection of the failed rubber-cord couplings stated that the cause of a failure was a partial circular rupture of the side surface at the point of attachment to the flange on the traction motor side. This type of damage was found in approximately 10 rubber-cord couplings. Examples of coupling damages are shown on (Figure 4).

Due to the fact that rupture of the side surface of a rubber-cord coupling is dangerous, the question arose of what are the causes and how to minimize it? To find the causes of the damage, 2 rubber-cord couplings were taken for research:

- removed from the motor car No 2022-02 (Figure 4a);
- removed from the motor car No 964-04 (Figure 4b).

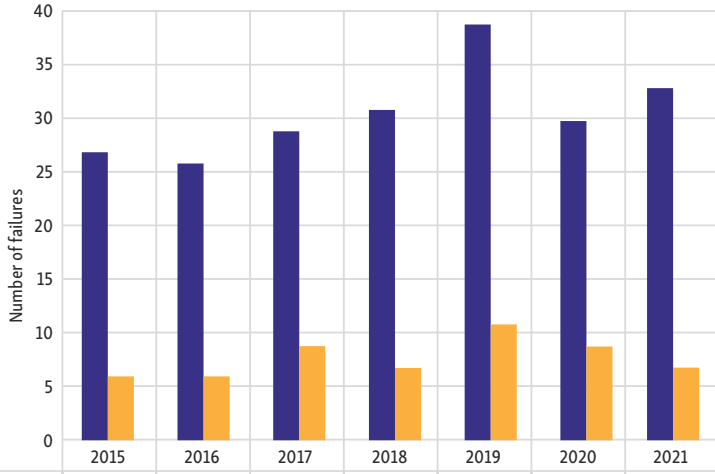

	2015	2016	2017	2018	2019	2020	2021
total quantity traction gear of the not plannet repairs of ER2 EMU trains	26	25	28	30	38	29	32
rubber-cord failure in traction gear of ER2 EMU trains	5	5	8	6	10	8	6

Figure 3. Number of unplanned repairs and rubber-cord damage in EMU traction gear (2015–2021)

Figure 4. Rubber-cord coupling damage:
(a) – motor car No 2022-02; (b) – motor car No 964-04

Table 1. Expenses for unscheduled repairs to replace the rubber-cord coupling

Rubber-cord coupling replacement	One unplanned repair for coupling replacement [€]	During 2021 [€]	During 7 years [€]
ER2	575	3450	24150
ER2T	594	2376	16632
DR1A	160	0	480

Table 2. Data on the operation of rubber-cord couplings

Motor car No	Date of the TR-3 repair	Date of coupling failure	Operating time of the coupling on the motor car [days]	Coupling mileage on the motor car [km]
2022-02	31/01/2019	07/06/2021	857	197450
964-04	31/03/2020	03/06/2021	429	64078

Information about the operation of rubber-cord couplings on the motor car is presented in Table 2.

As rubber-cord couplings have been produced in Russia, their parameters are taken in accordance with GOST 33188-2014 standard, with further validation of the results according to ISO 14691:2008, DIN 740-1:1986-08, DIN 740-2:1986-08 standards.

Thus in accordance with GOST 33188-2014 standard the mileage between failures shall be at least 200 thousands km. When analysing the statistical data of the JSC "Passenger train" (in Latvian: *AS "Pasažieru vilciens"*) unscheduled repairs and motor cars mileages reports (template PVR4) (AS PV 2021) it was found that the mileage to failure of rubber-cord couplings was on average:

- 2015 → 130.8 thousands km;
- 2016 → 106.3 thousands km;
- 2017 → 98.5 thousands km;
- 2018 → 88.3 thousands km;

- 2019 → 97.1 thousands km;
- 2020 → 163.2 thousands km;
- 2021 → 121.1 thousands km.

In the 7 year period (from 2015 till 2021), at the time of failure with a mileage of more than 200 thousands km, only 4 failures of rubber-cord couplings out of 47 couplings were detected, which is less than 10% of all coupling failures. One possible reason for the failure of rubber-cord couplings in the range of average mileage from 88.3 to 163.2 thousand km is their untimely replacement with new ones during the type TR-3 repair, and the installation of the couplings is carried out depending on their actual condition.

Another possible reason for the failure of the coupling is incorrect installation or incorrect adjustment of the inclination angle of the cord coupling during the type TR-3 repair. An example of incorrect installation of a rubber-cord coupling is shown on Figure 5 (arrows indicate an installation defect). Mileage from type TR-3 repair was 22742 km, defect detected during traction motor replacement on 08/12/2020.

An important condition for the reliable operation of the rubber-cord coupling is to prevent the warming of the rubber-cord shell above +75 °C under the action of the dynamic moment $M_d(t)$. The dynamic moment occurs when the rotational speed changes and is due to the forces of inertia of all moving elements of the traction drive without exception, as well as resulting from radial and angular displacements of the traction motor shafts and the traction gearbox connected by means of a rubber-cord coupling (Birjukov *et al.* 1986). Being under the motor car and located between the traction motor on one side and the traction gearbox on the other side, the rubber-cord coupling, in view of the limited space, in the summer season is subjected to additional heat from traction motors in traction mode, as well as wheelsets in braking mode. A large release of heat leads to warming of the outer shell of the coupling, resulting in its thermal aging. During thermal aging, almost all the main physical and mechanical properties of the material of the rubber-cord coupling change irreversibly throughout the entire volume (Levinson, Burgess 1971). In addition, as a result of temperature caused aging, the hardness of the outer surface layer of the rubber-cord coupling may change. To determine the temperature of the cord coupling in real operating conditions, on 04/07/2021, a trial trip was carried out on a 6 motor car ER2 series EMU train No 1307 on the Riga–Sloka–Riga line, the temperature was controlled using a contactless pyrometer *Raytek Raynger ST 20* with an accuracy class of ±1%, and the ambient air temperature was taken according to the information board at the Riga station. The results of measurements, the temperature of the outer shell of the rubber-cord coupling are shown in Table 3.

According to the results of a trial trip with the 50...60% occupancy of motor cars, the highest warming of the rubber-cord coupling of the 3rd wheelset was detected, which amounted to t = +43.1 °C. It is possible that under more severe operating conditions, such as the maximum occupancy of motor cars and ambient air temperature, which is more than t = +30 °C, then in these cases the temperature of the rubber-cord coupling can reach more than t = +60 °C. Therefore the condition of not allowing warming of the coupling higher than t = +75 °C is observed. Based on the results of temperature measurement and visual inspection of 12 rubber-cord couplings of the ER2 series EMU train No 1307, it was found out that there are signs of thermal aging, as well as in some places also the presence of small cracks on the side surface of the coupling (shown on Figure 6).

Figure 5. Motor car ER2 991-02 – incorrect installation of the rubber-cord coupling

Figure 6. Motor car No 991-06, appearance of the coupling from the side of the traction motor

Table 3. Determination of rubber-cord coupling temperature

Wheelset No	Air temperature at Riga station t_a [°C]	Coupling temperature t [°C] for motor car No		
		1307-02	991-06	1307-10
1	+27	+37.3	+41.5	+39.8
2		+39.7	+39.6	+38.4
3		+37.4	+43.1	+41.7
4		+42.6	+38.8	+39.1

The mileages of motor cars according to the reports (AS PV 2021) were:

- motor car No 991-06 → 185 thousands km;
- motor car No 1307-02 → 195 thousands km;
- motor No 1307-10 → 197 thousands km.

The research process of rubber-cord couplings consisted of 4 stages:

- the determination of the geometric dimensions of the coupling and comparison of the obtained data with the data of ISO 14691:2008;
- the theoretical determination (calculations) of: torque, centrifugal force, shear stress and radial load acting on the coupling;
- the determination of hardness on the Shore A (scale depending on the temperature of the rubber-cord coupling in temperature ranges t = –20 °C; 0 °C; +22 °C; +60 °C in the Riga Technical University (Latvia); comparison of the obtained data with the data of ISO 14691:2008;
- drawing the main conclusions and conclusions about the possible causes of the rupture of the rubber-cord coupling.

3.1. Determination of the geometric dimensions of a rubber-cord coupling

Stage 1 of the study consisted of determining the geometric dimensions of the coupling. To carry out this study, the rubber-cord couplings were removed from motor car No 2022-02 (Figure 7a) and motor car No 964-04 (Figure 7b) and fragments were cut out for research.

Measurements of the diameter of the outer surface of the coupling, the inner mounting surface diameter and the bead thickness were carried out using a calliper 0...550 mm with an accuracy class of 0.1 mm. The obtained measurement results were compared with the data of ISO 14691:2008 and are given in Table 4 and Figure 8.

To determine the value of shear stress τ_k, measurements of the side surface of the coupling were carried out using a 0...150 mm calliper with an accuracy class of 0.1 mm.

According to the results, it was found out that in the attachment of the rubber-cord coupling to the flanges of the traction motor, in the place where it breaks, the coupling has the following thickness of the side surface:

- from motor car No 2022-02 → $22.3^{+0.1}_{-0.1}$ mm.
- from motor car No 964-04 → $22.5^{+0.1}_{-0.1}$ mm.

The results of measuring the side surface of the couplings are shown on Figure 9.

3.2. Determination of forces acting on a rubber-cord coupling

At the Stage 2, the task was to determine the forces acting on the rubber-cord coupling. When calculating rubber-cord couplings, the initial data is the maximum torque that should not exceed 75% of the permissible buckling of the coupling shell (Birjukov *et al.* 1986). The buckling of a rubber-cord coupling is the inability of the coupling to maintain its original position or shape. According to Birjukov *et al.* (1986) loss of stability of the rubber-cord shells of couplings occurs at: $1.2 \cdot 10^4$ N·m. In this case, the permissible torque should not exceed $1.2 \cdot 10^4 \cdot 0.75 = 9 \cdot 10^3$ N·m (Birjukov *et al.* 1986). According to DIN 740-1:1986 standard, the maximum torque should not exceed $7.85 \cdot 10^3$ N·m (GOST 33188-2014; Krmela, Krmelova 2017). In suburban traffic conditions with short sections and frequent stops, the maximum torque M_a is achieved at low speeds of the traction motor during the acceleration of the EMU train.

Equation (1) defines the maximum torque M_a:

$$M_a = \frac{30 \cdot P}{\pi \cdot n} \cdot \eta , \quad (1)$$

where: P – traction motor power (P = 130 kW); π – is a mathematical constant; η – traction motor efficiency (according to Dunaev & Lelikov (1984), η = 86 ... 92%); n – traction motor speed [rpm] at speeds:

- 5 km/h → 64 rpm;
- 10 km/h → 129 rpm;
- 20 km/h → 258 rpm;
- 40 km/h → 517 rpm.

According to the calculation results, the torque M_a (assuming traction motor efficiency 90%) at speed:

- 5 km/h amounted to $1.74 \cdot 10^4$ N·m;
- 10 km/h amounted to $8.65 \cdot 10^3$ N·m;
- 20 km/h amounted to $4.32 \cdot 10^3$ N·m;
- 40 km/h amounted to $2.15 \cdot 10^3$ N·m.

According to the results of determining the torque M_a, it was stated that:

- at a speed of 5 km/h, the torque on the armature shaft, according to the calculations, is $1.74 \cdot 10^4$ N·m. At this torque value, the coupling becomes unstable, the coupling deforms with changes in geometric dimensions, which does not comply with the requirements DIN 740-2:1986 standard and exceeds the parameter by $9.5 \cdot 10^3$ N·m. Acceleration to a speed of 5 km/h according to the results of the test trial is an average of 2.5 s (Strautmanis *et al.* 2017);
- at 10 km/h, there is no buckling of the coupling shell. The condition for the loss of stability of the rubber-cord coupling shell (75%) is observed ($1.2 \cdot 10^4$ – 3000 (75%) = 9000 > $8.65 \cdot 10^3$). However, it does not meet the parameters of DIN 740-2:1986-08 standard and exceeds by $0.8 \cdot 10^3$ N·m. Acceleration to a speed of 10 km/h is an average of 5 s.

During operation, the following forces act on the rubber-cord coupling:

- centrifugal forces P_c, P_{c1};
- axial force F_a;
- lateral compression force T.

The high value of these forces can damage the rubber-cord coupling, graphic designation and moduli of the forces acting on the rubber-cord coupling are shown on Figure 10 (Savel'ev 1970).

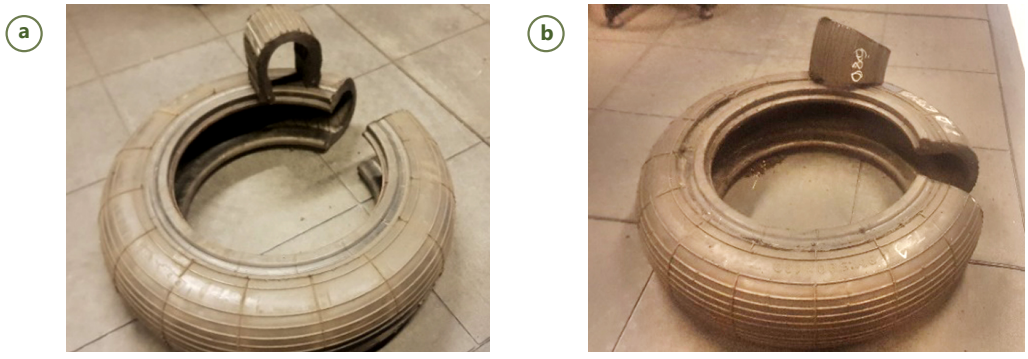

Figure 7. Preparation of the rubber-cord coupling for measurement:
(a) – motor car No 2022-02; (b) – motor car No 964-04

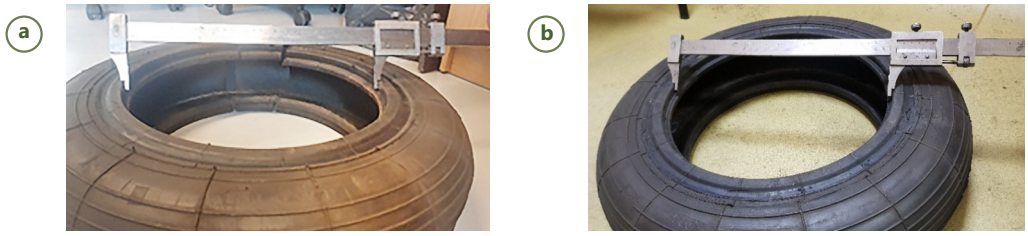

Figure 8. Measurements of the internal fitting diameter of the couplings:
(a) – motor car No 2022-02; (b) – motor car No 964-04

Figure 9. The measurement result of a fragment of the side surface of the coupling:
(a) – motor car No 2022-02; (b) – motor car No 964-04

Table 4. Determination of the geometric dimensions of the coupling

Measurement	Results of specimens measurements [mm] for motor car No		Parameters stated by ISO 14691:2008 [mm]
	2022-02	964-04	
Diameter of the outer surface of the coupling	$585.8^{+0.1}_{-0.1}$	$579.2^{+0.1}_{-0.1}$	$580.0^{+2.0}$
Inner diameter	$354.1^{+0.1}_{-0.1}$	$354.4^{+0,1}_{-0,1}$	$354.0^{+2.0}_{-2.0}$
Bead thickness	$28.7^{+0.1}_{-0.1}$	$29.4^{+0.1}_{-0.1}$	$30.0^{+2.0}_{-2.0}$

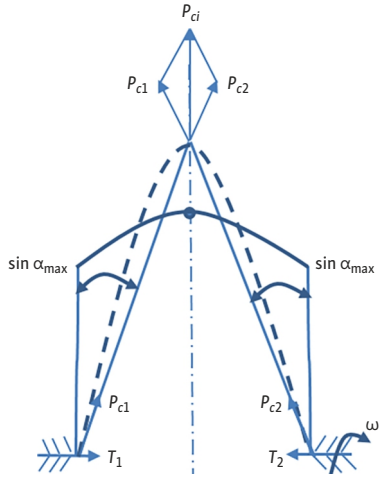

Figure 10. The action of forces on the rubber-cord coupling

Determination of the centrifugal forces P_c, P_{c1} (Figure 11). The data of the coupling parameters for performing the calculations were obtained as a result of measurements and have the following values and was determined for hourly operation mode and a maximum speed of 120 km/h (Freimane *et al.* 2016).

Coupling parameters:

- coupling diameter data D and inner diameter data d presented in Table 3;
- coupling top surface thickness δ (Figure 11): for motor car No 2022-02 δ = 0.0158 m, for motor car No 964-04 δ = 0.0165 m;

- coupling side thickness δ_1: for motor car No 2022-02 δ_1 = 0.0211 mm, for motor car No 964-04 δ_1 = 0.0213 mm;
- coupling width b: for motor car No 2022-02 b = 0.132 m, for motor car No 964-04 b = 0.131 m;
- density of the rubber-cord coupling $\rho = 1.2 \cdot 10^3$ kg/m^3;
- angular speed ω of the traction motor: in hourly mode $\omega = 119.9$ s^{-1}, at the speed of 120 km/h $\omega = 162.3$ s^{-1}.

Equation (2) defines the intensity of centrifugal force in the central part of the coupling q [N/m^2]:

$$q = \frac{dP_c}{ds} = \rho \cdot \delta \cdot \frac{D-\delta}{2} \cdot \omega^2 . \quad (2)$$

The intensity of the centrifugal force in the central part of the coupling q [N/m^2] is calculated (according to Equation (2)) provided that the elementary mass occupying the surface area ds is located at a radius $(D - \delta)/2$ and rotates with an angular velocity ω (Savel'ev 1970).

A similar approach was used when determining the centrifugal force on the side surfaces of the coupling (Equation (3)).

Equation (3) defines the intensity of centrifugal force in the side surface of the coupling q_1 [N/m^2]:

$$q_1 = \frac{dP_{c1}}{ds} = \rho \cdot \frac{D-d}{2} \cdot \frac{D+d}{2} \cdot \omega^2 . \quad (3)$$

Values of q and q_1 in hourly mode are:
- for motor car No 2022-02: $q = 7.778 \cdot 10^4$ N/m^2, $q_1 = 1.405 \cdot 10^6$ N/m^2;
- for motor car No 964-04: $q = 8.027 \cdot 10^4$ N/m^2, $q_1 = 1.372 \cdot 10^6$ N/m^2.

Values of q and q_1 at the speed of 120 km/h are:
- for motor car No 2022-02: $q = 1.486 \cdot 10^6$ N/m^2, $q_1 = 2.567 \cdot 10^6$N/m^2;
- for motor car No 964-04: $q = 1.471 \cdot 10^5$ N/m^2, $q_1 = 2.514 \cdot 10^6$ N/m^2.

Equation (4) defines the value of the elementary area of action of centrifugal force (Figure 12):

$$ds = \frac{D}{2} \cdot d\varphi \cdot dz . \quad (4)$$

Resultant specific centrifugal force acting on the coupling [N/m]. Figures 11 and 12 shows design diagrams of a cord coupling for determining centrifugal forces during its rotation at operating speeds (Savel'ev 1970).

Equation (5) defines the forces acting in the centre of the coupling P_c:

$$P_c = \int_0^{b-2\delta} q \, dz = \int_0^{b-2\delta} \rho \cdot \delta \cdot \frac{D-\delta}{2} \cdot \omega^2 \, dz = \rho \cdot \delta \cdot \frac{D-\delta}{2} \cdot \omega^2 \cdot (b - 2 \cdot \delta). \quad (5)$$

Values of P_c in hourly mode are:
- for motor car No 2022-02: $P_c = 7.809 \cdot 10^3$ N/m;
- for motor car No 964-04: $P_c = 7.95 \cdot 10^3$ N/m.

Values of P_c at the speed of 120 km/h are:
- for motor car No 2022-02: $P_c = 1.431 \cdot 10^4$ N/m;
- for motor car No 964-04: $P_c = 1.441 \cdot 10^4$ N/m.

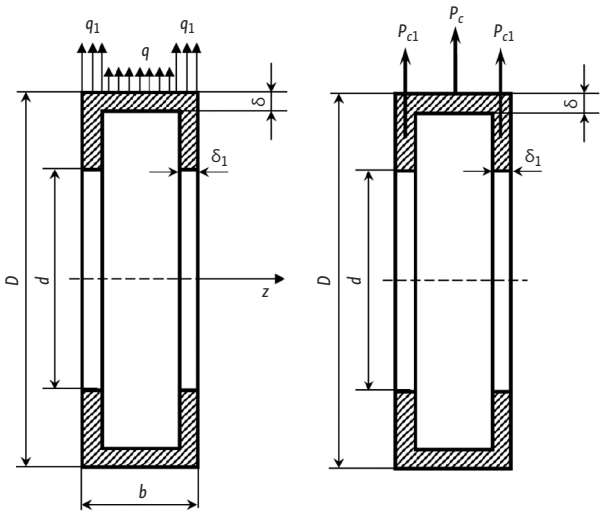

Figure 11. Centrifugal force acting on the coupling and its intensity

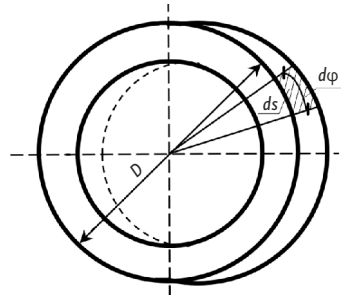

Figure 12. The value of the elementary area of action of centrifugal force

Equation (6) defines the forces acting in the lateral surface:

$$P_{c1} = \int_0^{\delta_1} q_1 \, dz = \int_0^{\delta_1} \rho \cdot \frac{D^2 - d^2}{4} \cdot \omega^2 \cdot d \, dz = \rho \cdot \frac{D^2 - d^2}{4} \cdot \omega^2 \cdot d \cdot \delta. \quad (6)$$

Values of P_{c1} in hourly mode are:
- for motor car No 2022-02: $P_{c1} = 1.055 \cdot 10^4$ N/m;
- for motor car No 964-04: $P_{c1} = 1.066 \cdot 10^4$ N/m.

Values of P_{c1} at the speed of 120 km/h are:
- for motor car No 2022-02: $P_{c1} = 1.933 \cdot 10^4$ N/m;
- for motor car No 964-04: $P_{c1} = 1.953 \cdot 10^4$ N/m.

Determination of the axial forces F_a acting on the rubber-cord coupling. Axial forces are forces that tend to compress the coupling and are directed, along it, the same axial forces act on the support bearings of the small gear and are sources of vibration and noise. Equation (7) defines the axial forces F_a:

$$F_a = 0.57 \cdot M_a - 0.22 \cdot 10^{-3} \cdot n^2, \quad (7)$$

where: n – traction motor speed [rpm] at speeds:
- 10 km/h → 129 rpm;
- 20 km/h → 258 rpm;
- 40 km/h → 517 rpm.

Force F_a [N] was determined at speeds:

- 10 km/h → $F_a = 4.92 \cdot 10^3$ N;
- 20 km/h → $F_a = 2.44 \cdot 10^3$ N;
- 40 km/h → $F_a = 1.16 \cdot 10^3$ N.

Determination of lateral compression force T. The appearance of specific lateral compression forces T is explained by the phenomena that at a high speed of 120 km/h, under the action of centrifugal force P_{c1}, the shell of the rubber-cord coupling is deformed in such a way that its side surfaces take on a conical shape (in Figure 10 the conical shape is shown by dashed lines). Equation (8) defines the lateral compression force T:

$$T = P_{c1} \cdot \sin\alpha. \tag{8}$$

Compression force T at a speed of 120 km/h:

- for motor car No 2022-02: $T = 2.686 \cdot 10^3$ N/m;
- for motor car No 964-04: $T = 2.714 \cdot 10^3$ N/m.

The value of $\sin\alpha_{max}$ was determined graphically taking into account the calculation of the centrifugal force, which increases with increasing speed (at a maximum speed of 120 km/h), graphically determined by the method $\alpha_{max} = 8°$; $\sin 8° = 0.139$ (Figure 10).

The torque on the shell of the rubber-cord coupling is transmitted by friction forces created by tightening the M24 bolts for fastening the rubber-cord coupling (Yatsun *et al.* 2020). When transmitting torque from the traction motor, the coupling, together with the coupling fastening to the flange, is subjected to a tangential torsional shear stress τ_k. The highest value of shear stress τ_k is achieved in the circular section at the flan clamp with a diameter D_1, during the acceleration of the EMU train, when the greatest (maximum) torque M_a is realized by the traction motor Figure 13.

As a next step, the torsional and shear stresses were determined. With this type of deformation, only torque acts in the cross sections of the coupling, as well as friction forces in the coupling Figure 14 (Feodos'ev 1999).

Coupling flange measurements are shown in Table 4.

Equation (9) defines the tangential torsional shear stress relative to friction point (Feodos'ev 1999):

$$\tau = \frac{M_a}{\frac{\pi \cdot D^4}{32} \cdot \left(1 - \frac{d^4}{D^4}\right)} \cdot \rho \ . \tag{9}$$

Equation (10) defines shear stress of the coupling relative to the coupling mounting flange (Feodos'ev 1999):

$$\tau_k = \frac{M_a}{\frac{\pi \cdot D^4}{32} \cdot \left(1 - \frac{d^4}{D^4}\right)} \cdot \frac{D}{2} = \frac{16 \cdot M_a}{\pi \cdot D^3 \cdot \left(1 - \frac{d^4}{D^4}\right)} \le [\tau], \tag{10}$$

where: $[\tau]$ – allowable shear stress (according to Dunaev & Lelikov (1984): 0.7...0.75 MPa).

Tangential shear stress τ relative to the coupling attachment point (Krmela, Krmelova 2017):

- at $M_a = 8.65 \cdot 10^3$ N·m: for motor car No 2022-02 $\tau = 0.86$ MPa, for motor car No 964-04 $\tau = 0.862$ MPa;
- at $M_a = 4.32 \cdot 10^3$ N·m: for motor car No 2022-02 $\tau = 0.427$ MPa, for motor car No 964-04 $\tau = 0.430$ MPa;
- at $M_a = 2.15 \cdot 10^3$ N·m: for motor car No 2022-02 $\tau = 0.212$ MPa, for motor car No 964-04 $\tau = 0.214$ MPa.

Shear stress of torsional shear τ_k of the coupling relative to the coupling mounting flange:

- at $M_a = 8.65 \cdot 10^3$ N·m: for motor car No 2022-02 $\tau_k = 1.028$ MPa, for motor car No 964-04 $\tau_k = 1.035$ MPa;
- at $M_a = 4.32 \cdot 10^3$ N·m: for motor car No 2022-02 $\tau_k = 0.513$ MPa, for motor car No 964-0 $\tau_k = 0.517$ MPa;
- at $M_a = 2.15 \cdot 10^3$ N·m: for motor car No 2022-02 $\tau_k = 0.255$ MPa, for motor car No 964-04 $\tau_k = 0.257$ MPa.

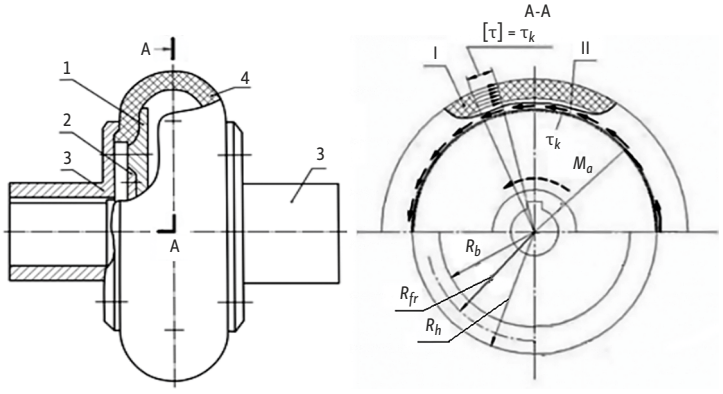

Figure 13. Fastening scheme and forces acting on the rubber-cord coupling:
1 – inner flange for fastening the rubber-cord coupling;
2 – connecting ring;
3 – flange on the side of the traction motor and traction gearbox;
4 – rubber-cord coupling;
τ_k – torsional shear stress; R_b – inner radius of the ring; R_{fr} – friction radius; R_h – ring outer radius

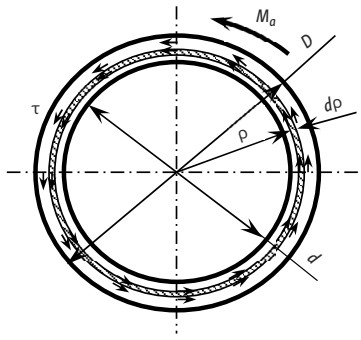

Figure 14. Calculation model for determining shear stress

According to the results of calculations, it was found that the maximum shear stress of torsional shear is achieved at the moment of starting the EMU train at a speed of 10 km/h $\left(M_a = 8.65 \cdot 10^3 \text{ N} \cdot \text{m}\right)$ for a coupling with motor car No 2022-02 is 1.028 MPa, while the allowable shear stress exceeded by 0.278 MPa; for coupling with motor car No 964-04 is 1.035. MPa, and exceeds the allowable shear stress by 0.285 MPa; at a speed of 20 km/h $\left(M_a = 4.32 \cdot 10^3 \text{ N} \cdot \text{m}\right)$, the allowable shear stress is not exceeded and amounts to motor car No 2022-02 is 0.513 MPa; motor car No 964-04 is 0.517 MPa.

Also, during the transportation of a large number of passengers in the motor car (during morning and evening peaks, as well as in the summer season), the weight of the motor car increases, as a result of which the traction motor shaft is displaced in relation to the shaft of the small gear of the gearbox, the coupling compensates misalignment of the shafts and, as a result, an additional radial load F_r appears in the coupling material (Mezitis *et al.* 2019).

Equation (11) defines the radial load F_r:

$$F_r = \left(0.1...0.3\right) \cdot F_r', \tag{11}$$

where: F_r' is the circumferential force on the coupling shell.

Equation (12) defines the circumferential force on the coupling shell:

$$F_r' = \frac{2000 \cdot M_a}{D}, \tag{12}$$

where: D – coupling diameter measured:

- for motor car No 2022-02 → 0.5865 m;
- for motor car No 964-04 → 0.5805 m

Circumferential force F_r' on the coupling shell:

- at 10 km/h: for motor car No 2022-02; $F_r' = 2.95 \cdot 10^7$ N, for motor car No 964-04 $F_r' = 2.98 \cdot 10^7$ N;
- at 20 km/h: for motor car No 2022-02; $F_r' = 1.47 \cdot 10^7$ N, for motor car No 964-04 $F_r' = 1.48 \cdot 10^7$ N;
- at 40 km/h: for motor car No 2022-02; $F_r' = 7.33 \cdot 10^6$ N, for motor car No 964-04 $F_r' = 7.48 \cdot 10^6$ N.

Radial load F_r:

- at 10 km/h: for motor car No 2022-02; $F_r = 5.89 \cdot 10^6$ N, for motor car No 964-04 $F_r = 5.96 \cdot 10^6$ N;
- at 20 km/h: for motor car No 2022-02; $F_r = 2.94 \cdot 10^6$ N, for motor car No 964-04 $F_r = 2.97 \cdot 10^6$ N;
- at 40 km/h: for motor car No 2022-02; $F_r = 1.46 \cdot 10^6$ N, for motor car No 964-04 $F_r = 1.48 \cdot 10^6$ N.

3.3. Determination of the hardness of a rubber-cord coupling

At the Stage 3, studies were carried out to determine the hardness of the rubber-cord coupling according to the "Shore A" scale ISO 14691:2008 depending on temperature. The coupling temperature measurements were not made by chance, since the rubber-cord coupling operates in a wide temperature range. Accordingly, the following temperatures were taken for research:

- t = +60 °C;
- t = +22 °C;
- t = 0 °C;
- t = –20 °C.

This study was aimed to identify how the temperature impacts the condition of rubber and its quality.

The obtained hardness measurement data were compared with the data of ISO 14691:2008. The measurement results are shown in Table 5.

Based on the obtained measurement results, it was found:

- at a temperature of –20 °C, both couplings, for all average measurement values, exceed the hardness parameters by 10.2...12.3 units, according to ISO 14691:2008;
- at a temperature of 0 °C, both couplings, for all average measurement values, exceed the hardness parameters by 0.7...7.3 units, according to ISO 14691:2008;
- at temperature +22 °C:
  - for the coupling from the motor car No 964-04 at all average measurement values, exceed the hardness parameters by 2.9...4.8 units according to ISO 14691:2008;
  - for the coupling from the motor car No 2022-02, 2 average measurement values exceed the hardness parameters by 0.2...1.5 units according to ISO 14691:2008;
- at a temperature of +60 °C, both couplings do not exceed the hardness values.

Since the failure of both couplings occurred in the summer season, when the coupling shell heats up more than t = +22 °C, at this temperature, the hardness on the side of the traction motor, i.e., in the place where the coupling breaks, slightly exceeds the parameters of ISO 14691:2008. A slight overestimated hardness, according to the authors, is not the reason for the rupture of the side surface of the coupling.

Table 4. Coupling flange measurement data

Motor car No	Outer ring diameter D [mm]	Ring inner diameter d [mm]	Place of attaching the coupling to the flange, friction diameter ρ [mm]	Friction diameter pad dp [mm]
2022-02	421.1	340.2	175.3	15.1
964-04	420.2	339.9	175.1	15.0

Table 5. Determination of the hardness of the rubber-cord coupling specimen

Place	Shore A hardness for rubber [units]								
	Average hardness for motor car No								ISO 14691:2008
	2022-02				964-04				
	t = +60 °C	t = +22 °C	t = 0 °C	t = –20 °C	t = +60 °C	t = +22 °C	t = 0 °C	t = –20 °C	
Side A* top	59.2	63.5	69.5	75.2	60.4	68.7	73.4	77.3	50.0...65.0
Side A middle	55.8	65.2	65.7	71.9	61.9	69.8	72.1	72.5	50.0...65.0
Side A bottom	59.1	64.6	71.1	73.5	62.1	69.2	74.1	75.9	50.0...65.0
Side B** top	60.2	65.8	72.3	74.1	58.7	67.9	70.4	73.6	50.0...65.0
Side B middle	61.5	62.1	68.4	72.9	62.4	68.4	72.3	74.9	50.0...65.0
Side B bottom	60.7	63.7	69.7	73.2	63.5	69.1	71.9	74.2	50.0...65.0

Notes: *side A – on the side of the gearbox; **side B – traction motor side.

4. Results and discussion

4.1. Possible reasons for the failure of the motor car No 2022-02 coupling

The failure of the motor car No 2022-02 rubber-cord coupling occurred when the coupling reached a mileage of more than 195 thousands km. With such mileage, the coupling has almost completely exhausted its service life of 200 thousands km. An external examination of the coupling revealed the presence of signs of thermal aging, as well as the presence of a large number of cracks on the side surface. A possible reason for the rupture of the side surface is the deformation of the rubber-cord coupling from a large periodic impact of the torque M_a and shear stress of torsional shear τ_k, which, with other unfavourable concomitant factors, led to a rupture of the side surface of the coupling.

In addition, the failure of the coupling removed from motor car No 2022-02 occurred in the summer season, when there is a large passenger load, the 2nd alleged reason for the failure of that coupling was the long-term effect of the radial load F_r on the material of the rubber-cord coupling. A larger value of the radial load F_r leads to stretching of the lateral surface, an increase in the size of the coupling and, accordingly, to a rupture of the lateral surface of the rubber-cord coupling. The large value of the radial load is confirmed by the results of measuring the diameter of the coupling, as a result of which, a discrepancy between the outer diameter of the coupling by 3.8 mm and the parameter of ISO 14691:2008 was stated.

4.2. Possible reasons for the failure of the motor car No 964-04 coupling

Since the failure of the coupling removed from motor car No 964-04 occurred when the mileage reached 34 thousand km, the 1st reason for the failure of the coupling possibly is untimely replacement with a new one during the type TR-3 repair. When analysing the data of unscheduled repairs, it was found that in the period from the last type TR-3 repair performed in 09/2019 and until 03/2021, unscheduled repairs to the wheelset were not carried out. Accordingly, the installation of the coupling took place from another wheelset according to its actual condition based on visual inspection. It is also possible, that the installation of a new coupling occurred in violation of the repair rules while installing the rubber-cord coupling during the type TR-3 repair.

5. Conclusions

- before installing the coupling on the rolling stock, it is necessary to check its geometric parameters. In case of non-compliance with the standard, installation of the coupling on rolling stock is prohibited;
- at each scheduled repair, to inspect the rubber-cord coupling. If cracks or tears are found, to prohibit further use of this coupling;
- a prolonged operation of the rubber-cord coupling in the speed range from 0 to 5 km/h due to high torque, which can lead to unstable operation of the coupling, high centrifugal force and, as a result, lead to rupture of its side surface, shall be avoided;
- it is necessary periodically, once a quarter, to measure the hardness of rubber at different temperatures and compare with the standard values. If the hardness does not match, the rubber-cord coupling shall be replaced with a new one;
- the heating temperature of the rubber-cord coupling shall be checked in summer, winter and autumn-spring periods. The heating temperature of the rubber-cord coupling should not exceed +75 °C;
- since the cause of the failure is the rupture of the shell in the place of torsional shear, which occurs when the maximum torque Ma is presented, the authors propose in the future experimentally determine the angle of the coupling twist. In the event that the twist angle is exceeded the permissible value (according to ISO 14691:2008, the twist angle should not exceed 4°), it is necessary to provide measures limiting the coupling twist angle to 3.5°.
- to reduce the number of failures of the rubber-cord coupling, it is necessary to consider measures to strengthen the side wall of the coupling with a layer of cord up to 10 layers instead of 8, and increase the thickness of the side wall of the rubber-cord coupling to 24...25 m.

Acknowledgements

This work has been supported by the European Social Fund within the Project No 8.2.2.0/20/I/008 "Strengthening of PhD students and academic personnel of Riga Technical University and BA School of Business and Finance in the strategic fields of specialization" of the specific objective 8.2.2 "To strengthen academic staff of higher education institutions in strategic specialization areas" of the operational programme "Growth and employment".

The authors would like to thank Riga Technical University (Latvia), employees of the metallographic laboratory and the laboratory for the resistance of materials for supporting this research.

Author contributions

Dmitrijs Gorbacovs was responsible for manuscript writing and editing, data analysis, content planning.

Pavels Gavrilovs and *Guntis Strautmanis* was responsible for literature search, data collection and analysis, content planning.

Janis Eiduks and *Ali Arshad* was responsible for manuscript editing, content planning and research guidance.

Disclosure statement

Authors do not have any competing financial, professional, or personal interests from other parties.

References

Abdelsalam, A. A.; El-Sabbagh, S. H.; Mohamed, W. S.; Khozami, M. A. 2023. Studies on swelling behavior, mechanical and thermal properties of ternary rubber blend composites in the presence of compatibilizers, *Pigment & Resin Technology* 52(5): 614–623. https://doi.org/10.1108/PRT-02-2022-0020

Ahundov, V. M.; Lunev, V. P. 2011. Raschetnye i jeksperimental''nye icsledovanija rezinokordnyh obolochek vysokojelastichnyh muft, *Problemy obchysljuval'noi' mehaniky i micnosti konstrukcij* 17: 35–42. Available from Internet: https://pommk.dp.ua/index.php/journal/article/view/188 (in Russian).

AS PV. 2021. *Elektrovilcienu nobraukumu atskaite*. AS "Pasažieru vilciens" (AS PV), Rīga, Latvia. (in Latvian).

Birjukov, I. V.; Beljaev, A. I.; Rybnikov, E. K. 1986. *Tjagovye peredachi jelektropodvizhnogo sostava zheleznyh dorog*. Moskva: Transport. 256 s. (in Russian).

Cukalo, P. V.; Prosvirin, B. K. 1994. *Jekspluatacija jelektropoezdov*: *spravochnik*. Moskva: Transport. 383 s. (in Russian).

DIN 740-1:1986-08. *Antriebstechnik*; *Nachgiebige Wellenkupplungen*; *Anforderungen*, *Technische Lieferbedingungen*. (in German).

DIN 740-2:1986-08. *Antriebstechnik*, *Nachgiebige Wellenkupplungen*, *Begriffe und Berechnungsgrundlagen*. (in German).

Dunaev, P. V.; Lelikov, O. P. 1984. *Detali mashin*: *kursovoe proektirovanie*. Moskva: Vysshaja shkola 1984. 336 s. (in Russian).

Feodos'ev, V. I. 1999. *Soprotivlenie materialov*: *uchebnik dlja vuzov*. Moskva: Izdatel'stvo MGTU im. N. Je. Baumana, 592 s. (in Russian).

Freimane, J.; Mezitis, M.; Mihailovs, F. 2016. Maneuver movements' safety increase using maneuver locomotive identification and distance control, *Procedia Computer Science* 104: 375–379. https://doi.org/10.1016/j.procs.2017.01.148

GOST 33188-2014. *Mufty tjagovogo privoda motorvagonnogo podvizhnogo sostava*. *Rezinokordnye obolochki*. *Obshhie tehnicheskie uslovija* [Traction Drive Couplings of Railway Electrical Multiple Units. Rubber Cord Casings. General Specifications]. (in Russian).

Il'ichev, V. A.; Pen'kov, I. A.; Korneev, V. S., Korneev, S. A. 2015. Jeksperimental'nyj stend dlja issledovanija nagruzochnyh harakteristik rezinokordnoj ploskoj mufty, *Omskij nauchnyj vestnik* 3: 123–126. (in Russian).

Ischuka, O.; Lomotko, D.; Eiduks, J. 2020. Modelling of technology of disassembling and assembling of freight trains at marshalling yard, in *Transport Means 2020*: *Sustainability*: *Research and Solutions*: *Proceedings of the 24th International Scientific Conference*, 30 September – 2 October 2020, Kaunas, Lithuania, 1: 463–468.

Ischuka, O.; Lomotko, D.; Gavrilovs, P.; Freimane, J. 2019. Improvement of technology of operation for Daugavpils marshalling station by building the new receiving yard, in *Transport Means 2019*: *Sustainability*: *Research and Solutions*: *Proceedings of the 23rd International Scientific Conference*, 2–4 October 2019, Palanga, Lithuania, 2: 841–846.

ISO 14691:2008. *Petroleum*, *Petrochemical and Natural Gas Industries – Flexible Couplings for Mechanical Power Transmission – General-Purpose Applications*.

Korneev, V. S.; Romanyuk, D. A.; Korneev, S. A.; Russkih, G. S.; Vaskova, M. V. 2016. Finite element research of rubber-cord flat coupling, *Procedia Engineering* 152: 321–326. https://doi.org/10.1016/j.proeng.2016.07.710

Krmela, J.; Krmelova, V. 2017. Tire casings and their material characteristics for computational modeling of tires, in *Engineering for Rural Development*: *16th International Scientific Conference*, 24–26 May 2017, Jelgava, Latvia, 230–235. https://doi.org/10.22616/ERDev2017.16.N043

Levinson, M.; Burgess, I. W. 1971. A comparison of some simple constitutive relations for slightly compressible rubber-like materials, *International Journal of Mechanical Sciences* 13(6): 563–572. https://doi.org/10.1016/0020-7403(71)90042-7

Li, K.; Chen, Z.; Shi, W. 2022. Rubber aging life prediction based on interpolation and improved time-temperature superposition principle, *Materials Research Express* 9(1): 015301. https://doi.org/10.1088/2053-1591/ac45ba

Lou, W.; Xie, C.; Guan, X. 2023. Molecular dynamic study of radiation-moisture aging effects on the interface properties of nano-silica/silicone rubber composites, *Materials Degradation* 7: 32. https://doi.org/10.1038/s41529-023-00351-8

Mahutov, N. A.; Shheglov, B. A.; Evdokimov, A. P. 2005. Snizhenie dinamicheskoj nagruzhennosti i osobennosti raboty silovyh privodov dlja normal''nyh i vneshtatnyh uslovij, *Problemy mashinostroenija i nadezhnosti mashin* (2): 87–90. (in Russian).

Mezitis, M.; Panchenko, V.; Kutsenko, M.; Maslii, A. 2019. Mathematical model for defining rational constructional technological parameters of marshalling equipment used during gravitational target braking of retarders, *Procedia Computer Science* 149: 288–296. https://doi.org/10.1016/j.procs.2019.01.137

Muhitovs, R.; Mezitis, M.; Korago, I. 2020. Development of the railway point electric heating intellectual control algorithm, *Transport Problems* 15(1): 71–79. Available from Internet: http://transportproblems.polsl.pl/pl/Archiwum/2020/zeszyt1/2020t15z1_07.pdf

Pegov, D. V.; Burcev, P. V.; Andreev, V. E. 2003. *Jelektropoezda postojannogo toka*: *JeT2*, *JeT2M*, *JeR2T*, *JeD2T*. Moskva: Centr kommercheskih razrabotok, 184 s. (in Russian).

Savel'ev, I. V. 1970. *Kurs obshhej fiziki. Tom 1. Mehanika, kolebanija i volny, molekuljarnaja fizika*. Moskva: Nauka. 511 s. (in Russian).

Sheshenin, S. V.; Gritchenko, M. E.; Chistyakov, P. V. 2021. Averging the viscoelastic properties of a rubber-cord ply in a plane stress state, *Mechanics of Composite Materials* 57(4): 469–480. https://doi.org/10.1007/s11029-021-09970-1

Stojanović, V.; Deng, J.; Milić, D.; Petković, M. D. 2024. Dynamics of moving coupled objects with stabilizers and unconventional couplings, *Journal of Sound and Vibration* 570: 118020. https://doi.org/10.1016/j.jsv.2023.118020

Strautmanis, G.; Mezitis, M.; Strautmane, V. 2017. The impact of rotor elastic suspension settings on the acceleration of the automatic balancer compensating mass, *Vibroengineering Procedia* 14: 13–17. https://doi.org/10.21595/vp.2017.18306

VAS LD. 1997. *Elektrovilcienu tekošā remontu un tehniskas apkalpošanas noteikumi L31/97*. Valsts akciju sabiedrība "Latvijas dzelzceļš" (VAS LD), Rīga, Latvia. 152 lpp. (in Latvian).

Yatsun, V.; Filimonikhin, G.; Haleeva, A.; Krivoblotsky, L.; Machok, Y.; Mezitis, M.; Podoprygora, N.; Sadovyi, M.; Strautmanis, G. 2020. Searching for the twofrequency motion modes of a three-mass vibratory machine with a vibration exciter in the form of a passive auto-balancer, *Eastern–European Journal of Enterprise Technologies* 4(7): 103–111. https://doi.org/10.15587/1729-4061.2020.209269

Zhang, Z.; Pang, G.; Zheng, H.; Jiang, X.; Li, R. 2023. Failure characterization of silicone rubber in corrosive environments based on leakage current characteristics, *IEEE Transactions on Dielectrics and Electrical Insulation* 30(4): 1810–1818. https://doi.org/10.1109/TDEI.2023.3236596

Zhou, Z.; Hou, Z.; Guo, J.; Jia, J.; Liu, Z.; Zhao, F.; Li, Y.; Tan, S.; Xin, Z.; Zhao, S.; Li, L. 2023. Study on the fatigue resistance of natural rubber with SiO_2 microspheres, *Journal of Polymer Research* 30(8): 324. https://doi.org/10.1007/s10965-023-03704-8